Selective antimony reduction initiating the nucleation and growth of InSb quantum dots

Crisp, Ryan W.; Grimaldi, Gianluca; De Trizio, Luca; Evers, Wiel H.; Kirkwood, Nicholas; Kinge, Sachin; Manna, Liberato; Siebbeles, Laurens D.A.; Houtepen, Arjan J.

DOI
10.1039/c8nr02381f

Publication date
2018

Document Version
Final published version

Published in
Nanoscale

Nanoscale

PAPER

View Article Online
View Journal | View Issue

Cite this: *Nanoscale*, 2018, **10**, 11110

Selective antimony reduction initiating the nucleation and growth of InSb quantum dots†

Ryan W. Crisp, [a] Gianluca Grimaldi, [a] Luca De Trizio,[b] Wiel H. Evers, [a,c] Nicholas Kirkwood, [a] Sachin Kinge,[d] Liberato Manna,[a,b,c] Laurens D. A. Siebbeles [a] and Arjan J. Houtepen*[a]

Received 22nd March 2018,
Accepted 25th May 2018

DOI: 10.1039/c8nr02381f

rsc.li/nanoscale

Indium antimonide (InSb) quantum dots (QDs) have unique and interesting photophysical properties, but widespread experimentation with InSb QDs is lacking due to the difficulty in synthesizing this material. The key experimental challenge in fabricating InSb QDs is preparing a suitable Sb-precursor in the correct oxidation state that reacts with the In-precursor in a controllable manner. Here, we review and discuss the synthetic strategies for making colloidal InSb QDs and present a new reaction scheme yielding small (~1 nm diameter) InSb QDs. This was accomplished by employing $Sb(NMe_2)_3$ as the antimony precursor and by screening different reducing agents that can selectively reduce it to stibine *in situ*. The released SbH_3, subsequently, reacts with In carboxylate to form small InSb clusters. The absorption features are moderately tunable (from 400 nm to 660 nm) by the amount and rate of reductant addition as well as the temperature of injection and subsequent annealing. Optical properties were probed with transient absorption spectroscopy and show complex time and spectral dependencies.

Introduction

Colloidal quantum dots (QDs) are size-tunable optoelectronic materials, with potential for use as light emitters, photodetectors, and solar cells.[1,2] However, the presence of toxic elements in commonly used QD materials, *e.g.* CdE (E = S, Se or Te) and PbE, limits their application, and prompts the development of less-toxic QD materials retaining favorable optical properties.[3] Indium-based III–V materials are promising candidates. For instance, InP QDs have tunable emission wavelengths and high photoluminescence quantum yield (PLQY) throughout the visible portion of the spectrum which could replace CdSe QDs in many applications.[3–5] Promising results with InAs QDs have recently shown emission in the near-infrared (NIR) with photoluminescence linewidths of 100–200 nm and modest PLQY of 5–20% for core/shell structures.[6,7] Continuing down the pnictogen column of the periodic table, InSb is a narrow bandgap semiconductor material offering favorable optoelectronic properties. Due to a large exciton Bohr radius of 54 nm, InSb QDs are in the strong confinement regime throughout the typical size range (2–20 nm) achieved in colloidal QD syntheses.[8,9] This property should allow facile control over the material bandgap *via* a small variation in QD size. The electron effective mass of bulk InSb is $0.0155m_0$ and the hole effective mass is $0.41m_0$, resulting in the highest electron mobility (78 000 $cm^2\ V^{-1}\ s^{-1}$) for bulk semiconductors, thereby making InSb QDs an interesting candidate to replace lead chalcogenide QDs for infrared photodetector applications and solar cells.[8–12] In particular, InSb QDs are promising for carrier multiplication (CM), a process in which a single absorbed photon generates multiple electron–hole pairs.[13,14]

Colloidal syntheses of InSb QDs have been previously demonstrated, but controlling the QD size over large ranges remains challenging and exhibits many barriers to widespread use among research groups. One particular challenge lies in finding a suitable Sb precursor for the colloidal synthesis of InSb QDs. Here, we present a novel synthesis approach to form InSb QDs by making use of tris(dimethylamino) antimony ($Sb(NMe_2)_3$) that is reacted *in situ* with *n*-butyllithium. We associate the intermediate species formed to stibine gas (SbH_3), based on similar reactions in the literature.[15–19] The stibine gas subsequently reacts with indium-oleate to form InSb QDs. We demonstrate various ways to control the InSb QD size and use transient absorption spectroscopy to probe their optical properties. Before presenting the details of our synthetic approach we first discuss the existing InSb QD syntheses in literature.

[a]*Optoelectronic Materials Section, Faculty of Applied Sciences, Delft University of Technology, Van der Maasweg 9, 2629 HZ Delft, The Netherlands. E-mail: A.J.Houtepen@tudelft.nl*
[b]*Department of Nanochemistry, Istituto Italiano di Tecnologia (IIT), via Morego, 30, 16163 Genova, Italy*
[c]*Kavli Institute of Nanoscience, Delft University of Technology, Van der Maasweg 9, 2629 HZ Delft, The Netherlands*
[d]*Toyota Motor Europe, Materials Research & Development, Hoge Wei 33, B-1930 Zaventem, Belgium*

† Electronic supplementary information (ESI) available. See DOI: 10.1039/c8nr02381f

A difficulty in the synthesis of III–V QDs lies in finding suitable pnictide precursors. Commonly available pnictide precursors often react too quickly so there is no separation between the nucleation and growth regimes, thereby forming a polydisperse product.[20,21] For instance, in the first report of InSb QDs by Evans *et al.*,[22] no size control was presented and the absorption spectra of the NCs lacked clear excitonic features. Such InSb QDs were prepared by reacting tris(trimethylsilyl)antimony [$Sb(TMS)_3$] and In-stearate, where the tris(trimethylsilyl)antimony [$Sb(TMS)_3$] was prepared by reducing elemental Sb (with Na_3Sb as an intermediary before silylation with chlorotrimethylsilane). TMS-based precursors are widely used,[23–25] especially for the III–V QD systems;[21,26,27] unfortunately, $Sb(TMS)_3$ has issues with long-term stability and is pyrophoric (similar to $P(TMS)_3$). Therefore, alternative precursors are desired to facilitate the synthesis of high-quality InSb QDs.

A complication in the search for other, more suitable, pnictide precursors is that pnictogens often take on positive oxidation states and hence do not as easily react with positive metal ions to form III–V or II–V compounds; a trend evidenced by the reductive environment often utilized in III–V or II–V syntheses.[3,16,28,29] An example is the reaction between In-oleate and tris(dimethylamino) pnictides, where after heterolytic cleavage of the pnictide–nitrogen bond the electrons tend to stay on the nitrogen, leaving the pnictide in the +3 oxidation state.[16,21,30]

Recent work Hens *et al.* explores how aminophosphine and aminoarsine precursors require a reducing agent to form the corresponding InP or InAs QDs.[6,31] In the synthesis of InP QDs, the aminophosphine acts as both a reductant and oxidant where a portion of the reagent is reduced from P^{3+} to P^{-3} species by oxidizing another portion to P^{+5} (*i.e.* $4P^{3+} \leftrightarrows 3P^{5+} + P^{3-}$).[31] The same strategy fails for the aminoarsine precursor presumably because the +5 oxidation state of As is less favorable hindering its oxidation from the +3 state; however, the addition of 3 equivalents of aminophosphine reduces the As to form InAs QDs with minimal residual P content.[6] Instead of using an aminophosphine as the As reductant, Talapin *et al.*, in a similar reaction scheme, explored the use of diisobutylaluminum hydride for the preparation of InAs QDs by *in situ* production of arsine species.[32]

In order to circumvent such issues also applicable to Sb, many different approaches have been proposed, for example Liu *et al.*[33] used tris(bis(trimethylsilyl)amino)antimony [$((TMS)_2N)_3Sb$], $InCl_3$ in oleylamine, and $LiEt_3BH$ that "activates" (*i.e.* reduces) both the Sb and In precursors to highly reactive $In^{(0)}$ and $Sb^{(0)}$ species which, in turn, form InSb QDs. This reaction scheme produces InSb QDs with the sharpest excitonic optical features reported and were more fully characterized in follow-up studies by Chang *et al.*[9] and Wang *et al.*[34] However, there are complications with this synthetic approach. Size-selective precipitation was used to get a range of sizes with exciton peaks that spanned the NIR spectrum from ~1300 nm to ~1800 nm and it was necessary to remove unwanted side-products – *i.e.* (opto)electronically active species – of the reaction which could potentially include metallic In.

In a different approach, Maurice *et al.*[35] used SbH_3 (stibine – a highly toxic gas in which the Sb already has the correct formal charge state (−3)) which is reacted with In-myristate to form InSb QDs with a size-dispersion around 13%. Despite a narrower size-dispersion than Liu *et al.* (~15%), the nanocrystals made with this method showed featureless absorption spectra and have limited size control. The difficulty of having a temporally narrow burst of gaseous stibine perhaps limits the ability to tune the nucleation and growth regimes.

Yarema *et al.*[36] used tris(dimethylamino)antimony [$Sb(NMe_2)_3$] and indium tris(bis(trimethylsilyl)amide) [$In(N(TMS_3)_2)_3$]. The precursors thermally decompose to form InSb in the presence of an alkylamine or alkylphosphine, which perhaps plays a role in the heterolytic cleavage of the amino-antimony bond.[16] The reaction mechanism involves formation of $In^{(0)}$ and $Sb^{(0)}$ that further react to yield InSb. Interestingly, different crystal structures (either zinc blende or wurtzite) can be attained using this reaction scheme by changing the starting precursor ratios. However, size-control leading to pronounced exciton peaks at shorter wavelengths than ~1250–1500 nm remains challenging.

Using the same antimony precursor, $Sb(NMe_2)_3$ and $InCl_3$, Tamang *et al.*[37] found that $LiEt_3BH$ or *n*-butyl lithium could be used as reductants to form $In^{(0)}$ and $Sb^{(0)}$ species which, as suggested by Liu *et al.*,[33] readily form InSb QDs. However, the absorption spectrum of the resulting nanocrystals is featureless and size control is lacking.

It is desirable to minimize the potential by-products (for instance $In^{(0)}$; present in non-colloidal syntheses as well[38,39]) that could adversely affect the resulting product. In the synthetic approach we propose here, we combined the methodologies presented above but employed an In precursor that is chemically inert to the reducing agent used to "activate" the Sb precursor. In this way, the chemistry involved in the reaction is simplified and the chance to produce unwanted side-products is low unlike other reported approaches. Furthermore, we present initial evidence for growing the seeds *via* the addition of precursors with controlled reactivity.

Experimental

Indium acetate (99.99%), tris(dimethylamino) antimony ($Sb(NMe_2)_3$, 99.99%), 1-octadecene (ODE, 90%), oleic acid (OA, 90%), *n*-butylithium (BuLi, 1.6 M in hexanes), methyl acetate (anhydrous, 99.5%), hexane (anhydrous, 95%), lithium triethylborohydride (Superhydride, 1 M in TFH), were purchased from Sigma Aldrich and used as received. Sodium borohydride ($NaBH_4$, 99%) was purchased from Thermo Fischer and used as received.

General procedure for synthesis of InSb QDs

The synthesis of InSb is carried out using standard Schlenk line techniques. In a typical synthesis, 3 mmol of indium

acetate, 9 mmol of oleic acid and 10 mL of ODE are degassed under vacuum in a three-neck flask at 110 °C for 20 minutes, flushed with nitrogen three times and then reacted at 170 °C to form indium oleate ($In(OA)_3$). The resulting acetic acid is removed under vacuum at 110 °C for 1 hour. In the meanwhile, in a nitrogen-filled glovebox, 3 mmol of $Sb(NMe_2)_3$ is mixed with 2 mL ODE and loaded into a syringe. Separately, 3 mmol of BuLi is loaded into a syringe with the needle tip stuck into a rubber septum to prevent a reaction with air as it is brought out of the glovebox. Under flowing nitrogen, the ODE/In-OA mixture is heated to 160–170 °C and the Sb-precursor solution is injected followed, quickly, by the BuLi. Unless otherwise specified, after the injection, the temperature is increased to 180–190 °C for 3 minutes and, eventually, the reaction is quenched with a water bath. As 160 °C is above the boiling point of hexane and BuLi, the reaction boils and produces vapor so it is recommended to use a condenser column and have the needle tip of the BuLi immersed into the solution when injecting. The color of the clear solution is yellow immediately after the BuLi injection and turns orange, red, then brown over several seconds as InSb forms. The reaction product is brought into a glove box and purified by adding 10 mL of hexane and sufficient methyl acetate until the solution turns turbid, typically ~30 mL. It is then centrifuged at 4000 rpm for 5 minutes and the resultant pellet of InSb QDs is redispersed in hexane. The same conditions were used for the other reductants (as described in the results) except sodium borohydride ($NaBH_4$) does not dissolve in ODE but makes a slurry that can still be injected.

Transmission electron microscopy analysis

(HR-TEM) images were obtained from a JEOL-JEM 3200 FSC microscope operating at 300 kV. Energy dispersive X-ray (EDX) analysis was performed on a JEOL-JEM1400 plus microscope operating at 120 kV. InSb QDs were deposited on a copper TEM grid covered with a 3 nm thick carbon supporting layer.

X-ray diffraction measurements

(XRD) were performed on a PANalytical Empyrean X-ray diffractometer equipped with a 1.8 kW Cu Kα ceramic X-ray tube, PIXcel3D 2 × 2 area detector and operating at 45 kV and 40 mA. Specimens for the XRD measurements were prepared in a glovebox by dropping a concentrated NCs solution onto a quartz zero-diffraction single crystal substrate. The diffraction patterns were collected at ambient conditions using a parallel beam geometry and symmetric reflection mode.

Transient absorption spectroscopy

Pump–probe transient absorption (TA) measurements are performed using a Yb:KGW oscillator (Light Conversion, Pharos SP) to output 180 fs pulses with a 1028 nm wavelength, at a 5 kHz frequency. The pump beam is obtained by sending the fundamental beam through an Optical Parametric Amplifier (OPA) equipped with a second harmonic module (Light Conversion, Orpheus), performing non-linear frequency mixing and producing an output beam. A small fraction of the fundamental beam power is used to produce a broadband probe spectrum (450–1600 nm), by supercontinuum generation in a sapphire crystal. The pump beam is transmitted through a mechanical chopper operating at 2.5 kHz, allowing one every two pump pulses to be transmitted. Pump and probe beam overlap at the sample position with a small relative angle (~8°), with a relative time delay controlled by an automated delay-stage. After transmission through the sample, the pump beam is dumped while the probe is collected at a detector (Ultrafast Systems, Helios). The differential absorbance is obtained *via* $\Delta A = \ln(I_{on}/I_{off})$, where I is the light incident on the detector with either pump-on or pump-off. TA data are corrected for probe-chirp *via* a polynomial correction to the coherent artifact. Pump photon fluence was estimated by measuring with a thermopile sensor (Coherent, PS19Q) the pump beam transmission through a pinhole of 1 mm radius.

Results and discussion

In principle, the best way to synthesize InSb QDs would be the *in situ* production of Sb^{3-} species which could readily react with In^{3+} ions. This challenge can be overcome using a reducing agent which can selectively reduce the Sb precursor to Sb^{3-} while keeping In oxidized in the +3 state. Employing $Sb(NMe_2)_3$ as the Sb precursor, in which Sb has a formal oxidation state of +3, we have explored various reducing agents to activate the nucleation of InSb QDs. We first try using $NaBH_4$ which leads to the formation of Sb^0 particles indicating that it does not have a strong enough reduction potential; *i.e.* the Sb^{3+} precursor is reduced to Sb^0 and not to Sb^{3-} (see Fig. 1, black curve). On the other extreme, superhydride ($Li[C_2H_5]_3BH$ – a powerful reductant) forms Sb^0, InSb, and In^0 particles when

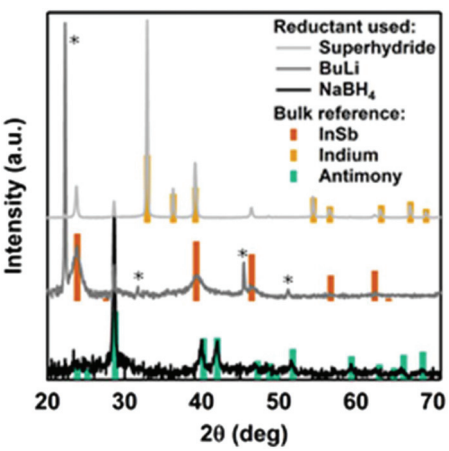

Fig. 1 XRD diffraction patterns of the synthetic product using three different reductants of varying strength. The bulk reflections of InSb (ICSD #640424), In (ICSD #109033) and Sb (ICSD #64696) are reported by means of brown, orange and green bars, respectively. The sharp peaks marked with asterisks in the InSb pattern match well to $In(OH)_3$ (JCPDS card 85-1338).

employed in the synthesis (see Fig. 1, light grey curve). BuLi appears to have intermediate reducing power as it does not react with $In(OA)_3$ but does react with $Sb(NMe_2)_3$. Control experiments indicate no visible reaction between the $Sb(NMe_2)_3$ and the $In(OA)_3$ (in the absence of BuLi) unless heated to ~270 °C where a gray solution forms. Furthermore, injecting BuLi without the $Sb(NMe_2)_3$ yields no visible reaction. Injecting $Sb(NMe_2)_3$ and BuLi into hot ODE (without $In(OA)_3$) yields an orange solution and black precipitate of Sb^0, as evidenced by XRD (see ESI Fig S1†) and observed by Tamang *et al.*[37]

Fig. 1 shows the XRD patterns of the materials produced by using the three reductants described. We find that only using BuLi results in the selective production of InSb nanoparticles. The proposed reaction mechanism is that BuLi undergoes a β-hydride elimination reaction with the $Sb(NMe_2)_3$ to produce stibine *in situ* which is known to react with $In(OA)_3$ to yield InSb,[35,38] as given in the following reactions:

$$Sb(NMe_2)_3 + 3C_4H_9Li \rightarrow SbH_3 + 3LiNMe_2 + 3C_4H_8$$

$$In(OA)_3 + SbH_3 \rightarrow InSb + 3H\text{-}OA$$

Quickly injecting 3 molar equivalents of BuLi results in small particles shown in the TEM image in Fig. 2, that we identify as small InSb nanocrystals with an approximate diameter of ~1 nm and energy-dispersive X-ray spectroscopy (EDX) indicates both In and Sb present in the nanocrystals (see ESI Fig. S2†). The optical features of the resulting particles are shown in Fig. 2b. The absorption spectrum exhibits a clear shoulder around 650 nm, in line with the very small size of the QDs. Analyzing the QDs with XRD indicates a wurtzite crystal structure (see ESI Fig. S3†). Inductively coupled plasma mass spectrometry (ICP-MS) indicates an atomic ratio of 1.8 : 1 for In : Sb and only minimal residual Li (34 : 1 In : Li) for the sample shown in Fig. 2a, which supports the reaction mechanism proposed. We conclude that the overall reaction is successful to produce InSb QDs, but only of very small sizes. It appears that the nucleation rate of InSb QDs under these conditions is very high and after nucleation no, or very little, monomer is left for subsequent growth.

Attempts to control the size by adjusting the temperature resulted in featureless absorption spectra, common to InSb QDs (see ESI Fig. S4†), therefore, different methods for tuning the size are employed. Instead of one fast injection of 3 molar equivalents BuLi (as shown in Fig. 2), the BuLi was added in small amounts over the course of ~5 minutes to grow the QDs slowly as shown in Fig. 3a. This systematically leads to QDs with absorption features that shift from ~350 nm to ~450 nm, hence of even smaller sizes than obtained by the rapid injection of BuLi described above. Mass spectrometry of the resulting material shows an In/Sb ratio of 1.8 and only minimal Li incorporation which further supports the reaction mechanism proposed. No further redshift is observed upon increasing the amount of BuLi further than 9 mmol (*i.e.* a 3 molar equivalent BuLi : $Sb(NMe_2)_3$, see ESI Fig. S5†). Our XRD analysis revealed that the InSb NCs obtained with this procedure have a zinc-blend structure (see Fig. 1) with extra peaks that match well to $In(OH)_3$. This unwanted secondary product potentially formed as the very small QDs are very prone to react with humid air or can arise from the oleate ligands.[40,41] Furthermore, Yarema *et al.*[36] observed polymorphism in the crystal structure of InSb QDs by changing the relative ratios of In : Sb. Here changing the amount of injected BuLi also yields different crystal structures of the resulting InSb QDs.

A second method to grow the particles larger is to induce Ostwald ripening by heating the QDs in solution. Heating the growth solution above 205 °C leads to uncontrolled growth and side reactions that cause a grey precipitate to form, thereby limiting the range in which the size can be tuned with this

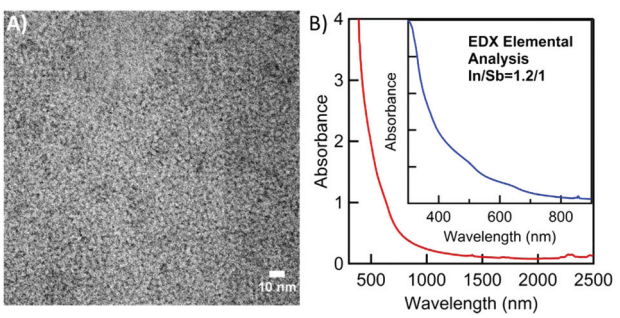

Fig. 2 (A) TEM image of small InSb QDs obtained by a fast injection of 3 molar equivalents of BuLi to Sb-precursor and (B) their absorption spectrum. An exciton feature is visible at 650 nm. The inset shows the results after 7 rounds of size-selective precipitation (see Fig. S7†) with clear features at 650 nm and 510 nm.

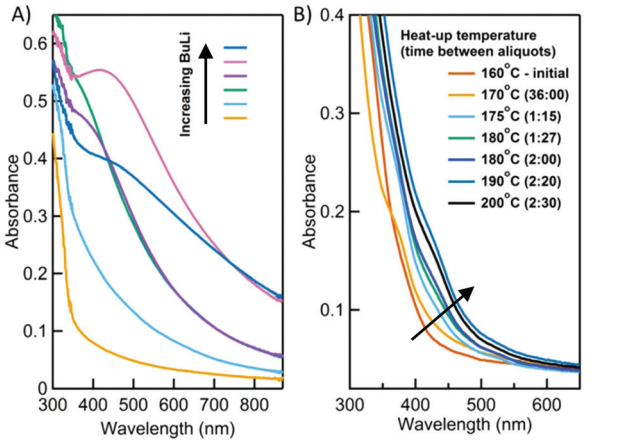

Fig. 3 Size tuning methods: (A) absorption spectra of aliquots taken as a function of added BuLi at 5 minutes intervals. The red-shift of the peak and absorption indicates larger InSb QD size. Mass spectrometry of the resulting material shows an In/Sb ratio of 1.8 and only minimal Li incorporation which further supports the reaction mechanism proposed. (B) Absorption spectra of InSb QDs heated to the temperature indicated with quantitative aliquots at the times given after the reaction mixture has reached temperature; for instance, the aliquot taken at 180 °C was removed from the mixture 1 minute and 27 seconds after the aliquot taken at 175 °C.

method. To avoid this, we isolated the QDs (made with 1 molar equivalent injection of BuLi) from their growth solution by flocculation and centrifugation, and then re-suspended them in ODE. Fig. 3b shows the absorption spectra of aliquots taken while heating these purified QDs to 200 °C. A gradual redshift of the QD absorption spectra is visible, indicating increasing QD size. In a separate experiment, the QDs were heated to 280 °C over the course of 10 minutes, but growth did not continue to shift the exciton peak to the red past 660 nm (Fig. S6†).

Finally, we attempted to grow the small InSb seed particles larger *via* multiple additions of extra precursors. Addition of $In(OA)_3$ and $Sb(NMe_2)_3$ without BuLi though does not lead to further growth, as expected. Therefore we decided to use a seeded growth approach by adding $In(N(TMS_3)_2)_3$ and $Sb(NMe_2)_3$, which are known to react without the need of a reductant,[36] to a solution of preformed InSb NCs (at a temperature lower than where nucleation is expected, *i.e.* ~130 °C). The addition of these precursors resulted in further growth of the small InSb seeds but significantly increased the width of the first exciton peak nm as shown in Fig. S6.†

The spectral features in Fig. 2 and 3 are relatively broad, as is commonly observed for InSb NCs. To probe whether the broad peaks are a result of size polydispersity or an inherent property of the QDs we performed size-selective precipitation by adding a small amount of methyl acetate, centrifuging, collecting the precipitate, then addition of more methyl acetate to the supernatant and repetition the process. The inset to Fig. 2b shows the resulting absorption spectrum after 7 rounds of such size selective precipitation. While the feature in the spectrum at ~520 nm and ~660 nm become clearer, they still remain quite broad. This suggest that much of the broadening of the spectral features is not caused by size polydispersity but, for instance, by crystal defects.

Furthermore, the QDs exhibit low photoluminescence (PL) intensity for the smaller sizes and no measureable PL for the larger sizes (Fig. S8†).[22,35,37] To get a better idea of the bandgap and exciton lifetime in these materials we, therefore, performed ultrafast transient absorption spectroscopy on the sample made by ripening/solvent annealing at 280 °C (shown in Fig. S6†) as it has the sharpest exciton peaks. Fig. 4a shows a 2D transient absorption image of the resulting change in absorption as a function of time and probe wavelength. Clear negative differential absorbance (bleach) features are observed at 520 nm and 660 nm, the same wavelengths where shoulders are visible in the absorption spectrum (see inset of Fig. 2B).[42] The multiple peaks are in line with the expected band structure for InSb, in which the valence band is split into a light hole, heavy hole, and spin–orbit split-off bands. We conclude that the lower energy bleach feature at 660 nm (or 1.8 eV) corresponds to the bandgap of the quantum dots. The higher energy transition potentially originates from the spin–orbit split-off band (as the energy difference is the same order of magnitude as in bulk (~0.8 eV)).[43] Alternatively, this transition could be due to a different point in the band structure (for instance, the L-point of the Brillouin zone) as suggested by the work from Sills *et al.*[8]

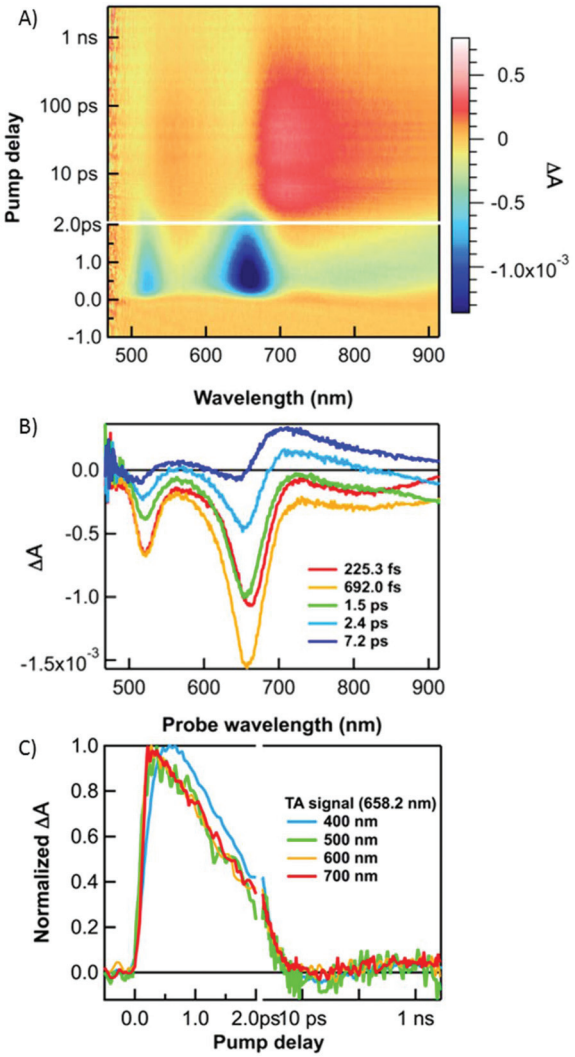

Fig. 4 (A) 2D transient absorption image showing the change in absorption (color coding) as a function of wavelength and time for InSb nanocrystals excited at 400 nm. (B) Spectral cuts at various times given in the legend showing the relative magnitudes of the bleach features at 660 nm and 520 nm. There is also photoinduced absorption developing at later times that obscures much of the bleach. (C) The time evolution of the bleach feature at probed at 660 nm at different excitation wavelengths, as indicated in the legend.

Fig. 4B shows spectral cuts at various delay times, while Fig. 4C shows transients of the bleach feature at 660 nm, obtained for different excitation wavelengths. It is clear that the lifetime of photoinduced charges is very short. After 7 ps the bleach features have disappeared and only a broad photoinduced absorption (PA) feature remains. Such a PA feature is often seen in QD samples with a low PL quantum yield (QY) and is often attributed to trapped charges.[44] The decay kinetics of the two bleach features are identical and excitation at a wavelength longer than 520 nm still results in a bleach of both features illustrating that they represent different optical transients involving the same species (Fig. S9†). This is expected for the transitions of various valence band states to a single con-

duction band state. We conclude that the decay of the absorption transients is caused by fast electron trapping. This is in line with the absence of PL and could indicate poor surface passivation, or potentially crystal defects in the QDs. Work is continuing on the origins of the short exciton lifetime, which is also observed for the particles made by Chang, Liu *et al.*[9]

In an attempt to improve the surface passivation (of the QDs shown in Fig. 3a) with a wide-bandgap material, a ZnTe shell growth procedure was carried out by adding zinc palmitate to the as-synthesized InSb cores, heating to 150 °C, and then dropwise addition of trioctylphosphine tellurium (TOP-Te). We chose ZnTe because Zn has been shown to increase the PLQY of InP and ZnTe is the most closely lattice-matched out of the Zn chalcogenides for which shell growth procedures are well-documented.[45,46] This treatment resulted in weak PL but worsened the absorption features as shown in Fig. S10.† One further complication is that at this QD size the PL observed is close in wavelength to the PL of neat $In(OA)_3$ and could potentially be related to ligand emission and not core QD particle emission.

It is still an open question why there are no exciton peaks in the absorption features of many III–V QDs. One possibility is that these materials contain many crystal defects obscuring the excitonic features due to shifts in the energy levels of optical transitions. A recent study on GaAs QDs shows that annealing QDs in molten salts can improve crystallinity, resulting in QDs exhibiting an exciton peak.[47] A similar effect could be present in InSb QDs synthesis, in which the low reaction temperatures might lead to vacancies and amorphous regions not detected in the TEM analysis.

Another open question is, why it is so difficult to control the size of InSb QDs with methods that are common for the synthesis of II–VI and IV–VI semiconductor QDs, such as changing the reaction temperature, inducing Ostwald ripening or using multiple injections of precursors.

Often the traditional synthesis methods for II–VI and IV–VI semiconductor QDs are based on the classical nucleation and growth theory originally developed by LaMer.[48] This theory depends on the equilibrium between monomers in solution or incorporated into a crystal. In the present case it appears as no such equilibrium exists perhaps because the back reaction where monomers re-dissolve is prevented. This would be the case if the Gibbs free energy of the solids state is much more negative than of the monomers in solution and would lead to a hit-and-stick process where, as soon as the monomers diffuse together, they react. If no equilibrium is established during the synthesis, it will be entirely kinetically driven and the concepts of nucleation and growth that are commonly used for II–VI and IV–VI QD synthesis do not apply.

Conclusions

We have investigated various reducing agents to be used in the synthesis of InSb QDs. We find *n*-butyl lithium to be the most suitable as it is able to selectively produce Sb^{3-} species without reducing the In precursor. More specifically BuLi leads to the *in situ* formation of stibine gas from tris(dimethylamino) antimony which can readily react with In^{3+} species to form small InSb QDs.

By controlling the injection conditions of the BuLi we make very small InSb clusters. Some limited size control is achieved with heating up or the addition of additional precursors that react without the need for an activating step. The crystal phase of the resulting material also changes based on the injection amount of BuLi, an effect also observed by Yarema *et al.*[36] The exciton lifetime, however, remains quite short, similar to the measurements of Chang *et al.*[9] Interestingly, in TA measurements, multiple bleach signals are present that could be related to different transitions in the band structure and warrants further exploration. Treating the QDs with Zn-stearate and TOP-Te in a shell growth procedure leads to improved PL. While control over the size and optical properties of the InSb QDs is still limited they could potentially serve as seed particles for the growth of larger InSb QDs similar to the work done on CdSe and InP.[49,50]

Conflicts of interest

There are no conflicts to declare.

Acknowledgements

RWC, GG, LDAS and AJH were supported by STW (project No. 13903, Stable and Non-Toxic Nanocrystal Solar Cells). AJH further acknowledges support from the European Research Council Horizon 2020 ERC Grant Agreement No. 678004 (Doping on Demand). LDT and LM acknowledge support from the European Research Council FP7 ERC Grant Agreement No. 614897 (TRANS-NANO). The authors thank Zeger Hens and Mickael Tessier for valuable discussions.

References

1 J. M. Pietryga, Y.-S. Park, J. Lim, A. F. Fidler, W. K. Bae, S. Brovelli and V. I. Klimov, *Chem. Rev.*, 2016, **116**, 10513–10622.
2 D. V. Talapin, J.-S. Lee, M. V. Kovalenko and E. V. Shevchenko, *Chem. Rev.*, 2009, **110**, 389–458.
3 P. Reiss, M. Carrière, C. Lincheneau, L. Vaure and S. Tamang, *Chem. Rev.*, 2016, **116**, 10731–10819.
4 F. Pietra, N. Kirkwood, L. De Trizio, A. W. Hoekstra, L. Kleibergen, N. Renaud, R. Koole, P. Baesjou, L. Manna and A. J. Houtepen, *Chem. Mater.*, 2017, **29**, 5192–5199.
5 F. Pietra, L. De Trizio, A. W. Hoekstra, N. Renaud, M. Prato, F. C. Grozema, P. J. Baesjou, R. Koole, L. Manna and A. J. Houtepen, *ACS Nano*, 2016, **10**, 4754–4762.
6 V. Grigel, D. Dupont, K. De Nolf, Z. Hens and M. D. Tessier, *J. Am. Chem. Soc.*, 2016, **138**, 13485–13488.
7 Y. W. Cao and U. Banin, *J. Am. Chem. Soc.*, 2000, **122**, 9692–9702.

8 A. Sills, P. Harrison and M. Califano, *J. Phys. Chem. Lett.*, 2016, **7**, 31–35.
9 A. Y. Chang, W. Liu, D. V. Talapin and R. D. Schaller, *ACS Nano*, 2014, **8**, 8513–8519.
10 D. L. Rode, *Phys. Rev. B: Solid State*, 1971, **3**, 3287–3299.
11 N. Bouarissa and H. Aourag, *Infrared Phys. Technol.*, 1999, **40**, 343–349.
12 E. O. Kane, *J. Phys. Chem. Solids*, 1957, **1**, 249–261.
13 V. I. Klimov, *J. Phys. Chem. B*, 2006, **110**, 16827–16845.
14 F. C. M. Spoor, G. Grimaldi, C. Delerue, W. H. Evers, R. W. Crisp, P. Geiregat, Z. Hens, A. J. Houtepen and L. D. A. Siebbeles, *ACS Nano*, 2018, **12**, 4796–4802.
15 R. C. Fischer, in *Encyclopedia of Inorganic and Bioinorganic Chemistry*, 2016, DOI: 10.1002/9781119951438.eibc0012.pub2.
16 M. A. Malik, M. Afzaal and P. O'Brien, *Chem. Rev.*, 2010, **110**, 4417–4446.
17 A. C. Jones and P. O'Brien, *CVD of Compound Semiconductors: Precursor Synthesis, Developmeny and Applications*, Wiley, 2008.
18 A. Kuczkowski, S. Fahrenholz, S. Schulz and M. Nieger, *Organometallics*, 2004, **23**, 3615–3621.
19 A. K. Gupta, *Detailed Project Profiles on 9 Selected Chemical Industries*, 2nd revised edn, 2014.
20 P. M. Allen, B. J. Walker and M. G. Bawendi, *Angew. Chem., Int. Ed.*, 2010, **49**, 760–762.
21 D. K. Harris and M. G. Bawendi, *J. Am. Chem. Soc.*, 2012, **134**, 20211–20213.
22 C. M. Evans, S. L. Castro, J. J. Worman and R. P. Raffaelle, *Chem. Mater.*, 2008, **20**, 5727–5730.
23 C. B. Murray, C. R. Kagan and M. G. Bawendi, *Annu. Rev. Mater. Sci.*, 2000, **30**, 545–610.
24 M. A. Hines and G. D. Scholes, *Adv. Mater.*, 2003, **15**, 1844–1849.
25 J. Zhang, R. W. Crisp, J. Gao, D. M. Kroupa, M. C. Beard and J. M. Luther, *J. Phys. Chem. Lett.*, 2015, **6**, 1830–1833.
26 S. Xu, S. Kumar and T. Nann, *J. Am. Chem. Soc.*, 2006, **128**, 1054–1055.
27 D. Franke, D. K. Harris, O. Chen, O. T. Bruns, J. A. Carr, M. W. B. Wilson and M. G. Bawendi, *Nat. Commun.*, 2016, **7**, 12749.
28 J. Lauth, T. Strupeit, A. Kornowski and H. Weller, *Chem. Mater.*, 2013, **25**, 1377–1383.
29 M. Green, *Semiconductor Quantum Dots: Organometallic and Inorganic Synthesis*, Royal Society of Chemistry, 2014.
30 M. Yarema, R. Caputo and M. V. Kovalenko, *Nanoscale*, 2013, **5**, 8398–8410.
31 M. D. Tessier, K. De Nolf, D. Dupont, D. Sinnaeve, J. De Roo and Z. Hens, *J. Am. Chem. Soc.*, 2016, **138**, 5923–5929.
32 V. Srivastava, E. M. Janke, B. T. Diroll, R. D. Schaller and D. V. Talapin, *Chem. Mater.*, 2016, **28**, 6797–6802.
33 W. Liu, A. Y. Chang, R. D. Schaller and D. V. Talapin, *J. Am. Chem. Soc.*, 2012, **134**, 20258–20261.
34 T. Wang, R. Vaxenburg, W. Liu, S. M. Rupich, E. Lifshitz, A. L. Efros, D. V. Talapin and S. J. Sibener, *ACS Nano*, 2015, **9**, 725–732.
35 A. Maurice, M. L. Haro, B. Hyot and P. Reiss, *Part. Part. Syst. Charact.*, 2013, **30**, 828–831.
36 M. Yarema and M. V. Kovalenko, *Chem. Mater.*, 2013, **25**, 1788–1792.
37 S. Tamang, K. Kim, H. Choi, Y. Kim and S. Jeong, *Dalton Trans.*, 2015, **44**, 16923–16928.
38 E. E. Foos, R. L. Wells and A. L. Rheingold, *J. Cluster Sci.*, 1999, **10**, 121–131.
39 Y. Li, Z. Wang, X. Duan, G. Zhang and C. Wang, *Adv. Mater.*, 2001, **13**, 145–148.
40 L.-T. Lin, L. Tang, R. Zhang, C. Deng, D.-J. Chen, L.-W. Cao and J.-X. Meng, *Mater. Res. Bull.*, 2015, **64**, 139–145.
41 F. Kaneko, K. Yamazaki, K. Kitagawa, T. Kikyo, M. Kobayashi, Y. Kitagawa, Y. Matsuura, K. Sato and M. Suzuki, *J. Phys. Chem. B*, 1997, **101**, 1803–1809.
42 G. Allan, Y. M. Niquet and C. Delerue, *Appl. Phys. Lett.*, 2000, **77**, 639–641.
43 A. L. Efros and M. Rosen, *Phys. Rev. B: Condens. Matter Mater. Phys.*, 1998, **58**, 7120–7135.
44 J. I. Saari, E. A. Dias, D. Reifsnyder, M. M. Krause, B. R. Walsh, C. B. Murray and P. Kambhampati, *J. Phys. Chem. B*, 2013, **117**, 4412–4421.
45 S. Xu, J. Ziegler and T. Nann, *J. Mater. Chem.*, 2008, **18**, 2653–2656.
46 W. M. Haynes, *CRC handbook of chemistry and physics*, CRC press, Boca Raton, Lodon, New York, 95th edn, 2014.
47 V. Srivastava, W. Liu, E. M. Janke, V. Kamysbayev, A. S. Filatov, C.-J. Sun, B. Lee, T. Rajh, R. D. Schaller and D. V. Talapin, *Nano Lett.*, 2017, **17**, 2094–2101.
48 G. M. Pound and V. K. L. Mer, *J. Am. Chem. Soc.*, 1952, **74**, 2323–2332.
49 S. L. Cumberland, K. M. Hanif, A. Javier, G. A. Khitrov, G. F. Strouse, S. M. Woessner and C. S. Yun, *Chem. Mater.*, 2002, **14**, 1576–1584.
50 D. C. Gary, M. W. Terban, S. J. L. Billinge and B. M. Cossairt, *Chem. Mater.*, 2015, **27**, 1432–1441.